Anal. Chem. **2010,** *82,* 808–816

Technique for Real-Time Measurements of Endothelial Permeability in a Microfluidic Membrane Chip Using Laser-Induced Fluorescence Detection

Edmond W. K. Young,[†,‡,#] Michael W. L. Watson,[§] Suthan Srigunapalan,[†,‡] Aaron R. Wheeler,[*,‡,§] and Craig A. Simmons[*,†,‡]

Department of Mechanical and Industrial Engineering, University of Toronto, 5 King's College Road, Toronto, Ontario, Canada, M5S 3G8, Institute of Biomaterials and Biomedical Engineering, University of Toronto, 164 College Street, Toronto, Ontario, Canada, M5S 3G9, and Department of Chemistry, University of Toronto, 80 St. George Street, Toronto, Ontario, M5S 3H6

Characterizing permeability of the endothelium that lines blood vessels and heart valves provides fundamental physiological information and is required to evaluate uptake of drugs and other biomolecules. However, current techniques used to measure permeability, such as Transwell insert assays, do not account for the recognized effects of fluid flow-induced shear stress on endothelial permeability or are inherently low-throughput. Here we report a novel on-chip technique in a two-layer membrane-based microfluidic platform to measure real-time permeability of endothelial cell monolayers on porous membranes. Bovine serum albumin (a model protein) conjugated with fluorescein isothiocyanate was delivered to an upper microchannel by pressure-driven flow and was forced to permeate a poly(ethylene terephthalate) membrane into a lower microchannel, where it was detected by laser-induced fluorescence. The concentration of the permeate at the point of detection varied with channel flow rates in agreement to less than 1% with theoretical analyses using a pore flow model. On the basis of the model, a sequential flow rate stepping scheme was developed and applied to obtain the permeability of cell-free and cell-bound membrane layers. This technique is a highly sensitive, novel microfluidic approach for measuring endothelial permeability in vitro, and the use of micrometer-sized channels offers the potential for parallelization and increased throughput compared to conventional shear-based permeability measurement methods.

Microfluidic devices have become useful analytical tools for chemical, biological, and biomedical studies. Many reports over the past decade have specifically demonstrated the utility of microfluidics for mammalian cell culture and cell-based assays.[1−4] Microfluidic dimensions and geometries are particularly well-suited for building cellular microenvironments tailored to mimic in vivo physiological conditions and for analyzing cellular behavior within these environments. Endothelial cells (ECs) constitute one cell type that benefits from the many advantages microfluidics has to offer. ECs cover all blood-contacting surfaces of the cardiovascular system, including the internal lining of blood vessels and the outer coating of heart valves. Because of their anatomic location, ECs are constantly exposed to hemodynamic shear stress generated by flowing blood. Shear stress is known to regulate many endothelial cell functions, and applying shear on ECs in in vitro systems is critical to the expression of certain EC responses.[5] Microfluidics not only offers lower reagent consumption, more options for geometries, and potential for parallelization, but also provides a platform well-suited for shear stress application on ECs in a manner analogous to macroscale parallel plate flow chambers.[6] Microfluidic devices have thus been used increasingly for shear-related EC experiments, including for studies on adhesion,[7] migration,[8] as well as for shear-induced nitric oxide production.[9]

A major function of the endothelium is selective trafficking of solutes and macromolecules from luminal blood to the tissue interstitium, and vice versa. Transport processes through the monolayer are tightly regulated by local chemical and mechanical microenvironments surrounding the cells and involve both trans-

* To whom correspondence should be addressed. E-mail: simmons@mie.utoronto.ca (C.A.S.); awheeler@chem.utoronto.ca (A.R.W.). Phone: 416-946-0548 (C.A.S.); 416-946-3864 (A.R.W.). Fax: 416-978-7753 (C.A.S.); 416-946-3865 (A.R.W.).

† Department of Mechanical and Industrial Engineering.

‡ Institute of Biomaterials and Biomedical Engineering.

§ Department of Chemistry.

Current location: Department of Biomedical Engineering, University of Wisconsin—Madison, Wisconsin Institutes for Medical Research, 1111 Highland Avenue, Madison, WI, 53705.

(1) Song, J. W.; Gu, W.; Futai, N.; Warner, K. A.; Nor, J. E.; Takayama, S. *Anal. Chem.* **2005**, *77*, 3993–3999.
(2) Genes, L. I.; Tolan, N. V.; Hulvey, M. K.; Martin, R. S.; Spence, D. M. *Lab Chip* **2007**, *7*, 1256–1259.
(3) Barbulovic-Nad, I.; Yang, H.; Park, P. S.; Wheeler, A. R. *Lab Chip* **2008**, *8*, 519–526.
(4) Paguirigan, A.; Beebe, D. J. *Integr. Biol.* **2009**, *1*, 182–195.
(5) Davies, P. F. *Physiol. Rev.* **1995**, *75*, 519–560.
(6) Young, E. W. K.; Simmons, C. A. *Lab on a Chip* **2010**, *10*, 143−160.
(7) Young, E. W. K.; Wheeler, A. R.; Simmons, C. A. *Lab Chip* **2007**, *7*, 1759–1766.
(8) Shamloo, A.; Ma, N.; Poo, M. M.; Sohn, L. L.; Heilshorn, S. C. *Lab Chip* **2008**, *8*, 1292–1299.
(9) Oblak, T. D.; Root, P.; Spence, D. M. *Anal. Chem.* **2006**, *78*, 3193–3197.

10.1021/ac901560w
Published on Web 01/05/2010

cellular and paracellular mechanisms.[10] These processes can be quantified by measuring the permeability of the endothelium, either as a transendothelial electrical resistance (TEER),[11−13] or via direct measurement of solute flux through the endothelial layer.[14,15] Endothelial permeability is widely studied because of its fundamental importance for understanding both physiological and pathological processes and its practical significance for determining pharmacokinetic properties of substances. Studying permeability helps characterize phenotypic differences between specific endothelial cell types, provides insight into developmental processes related to vascular disease progression,[16] and facilitates assessment of the ability of the vascular tissue lining to take up pharmaceutical drugs. Pharmacological properties are important for evaluating the efficacy of drugs and their suitability for public consumption.[17]

Currently, the majority of permeability assays are performed under static conditions where EC monolayers are cultured on membrane-based cell culture inserts and tagged molecules are allowed to permeate through the static monolayer on the luminal side and collect on the abluminal side.[17,18] Although static experiments are informative, and can permit high-throughput drug screening tests in well plate formats, they are not representative of the dynamic in vivo conditions where ECs are constantly exposed to shear stress. In particular, shear stress has been shown to effect changes in endothelial permeability.[19] For example, Sill and co-workers showed that when shear was applied to endothelium at 20 dyn/cm^2 for 4 h, permeability increased 4-fold compared to endothelium under static conditions.[14] This phenomenon is important from a pharmacological perspective because it suggests efficient and accurate assessment of drug efficacy depends not only on the ability to carry out high-throughput experiments but also on the ability to mimic the dynamic in vivo microenvironment. Without shear stress, in vitro model systems lack an important physical element of the in vivo condition that limits their applicability.

Flow systems have been used previously to study permeability of endothelial monolayers with shear stress,[14,19] but these systems were designed to test only one condition at a time. Some of these systems also required manual collection of samples that slows experimental procedure. There is a need for shear-based permeability systems that can potentially support in vivo-like drug screening for pharmacological applications at increased throughput. Microfluidics is well-suited for this application because of the advantages listed above. One recent report described a novel microfluidic system containing microholes to physically trap Caco-2 cells and measure drug permeability via transcellular transport.[20] Although this work clearly demonstrated the advantages of developing a microfluidic permeability assay, the design is not suitable for endothelial permeability because it does not accurately model para-endothelial transport mechanisms that act in concert with transcellular transport[10] or mechanical stimuli due to shear flow over the endothelium. A number of other reports have demonstrated the successful incorporation of membranes into microfluidic devices,[21−24] including a report on a device that can culture Caco-2 monolayers on membranes for over 2 weeks,[25] one describing a coculture between vascular endothelial cells and blood cells separated by a membrane,[2] and a recent study describing a device to measure endothelial monolayer permeability, but not under physiological shear flow conditions.[26] Membranes provide support for culturing endothelial monolayers while also allowing for molecular transport between regions separated by the membrane. Ultimately, membrane-based systems open the door for myriad biological lab-on-a-chip applications that could benefit from controlled channel-to-channel communication in a three-dimensional configuration where microchannels are permitted to pass above and below other neighboring microchannels.

Here, we present a novel real-time technique to measure biomolecule permeability across an endothelium monolayer cultured on a track-etched porous membrane separating two levels of microfluidic channels. Using laser-induced fluorescence (LIF) to detect fluorescently tagged bovine serum albumin (FITC−BSA) that permeated through the membrane region, we demonstrated the ability to measure endothelial permeability on a microscale platform. We chose BSA as a model protein because it is a commonly used molecule for studying vascular permeability and because serum albumin plays a vital role as a carrier protein for transport of hormones, fatty acids, and other molecules across the endothelium. The reported microfluidic system has the potential for parallelization, opening the door for physiologically relevant high-throughput drug screening capabilities.

EXPERIMENTAL SECTION

Microfluidic Device Design and Fabrication. A two-layer membrane-based microfluidic system was made from poly(dimethylsiloxane) (PDMS) (Sylgard 184, Dow Corning, Midland, MI) and consisted of north−south (top) and east−west (bottom) microchannels separated by a porous track-etched membrane (Figure 1A). The cross pattern of the microchannels formed a single intersection where molecular transport from one channel to the other was possible through the membrane. The design is similar to other membrane-incorporated microfluidic devices

(10) Mehta, D.; Malik, A. B. *Physiol. Rev.* **2006**, *86*, 279–367.
(11) Amerongen, G. P. V.; Draijer, R.; Vermeer, M. A.; van Hinsbergh, V. W. M. *Circ. Res.* **1998**, *83*, 1115–1123.
(12) Langeler, E. G.; Vanhinsbergh, V. W. M. *Thromb. Haemostasis* **1988**, *60*, 240–246.
(13) Rubin, L. L.; Hall, D. E.; Porter, S.; Barbu, K.; Cannon, C.; Horner, H. C.; Janatpour, M.; Liaw, C. W.; Manning, K.; Morales, J.; Tanner, L. I.; Tomaselli, K. J.; Bard, F. *J. Cell Biol.* **1991**, *115*, 1725–1735.
(14) Sill, H. W.; Chang, Y. S.; Artman, J. R.; Frangos, J. A.; Hollis, T. M.; Tarbell, J. M. *Am. J. Physiol.: Heart Circ. Physiol.* **1995**, *37*, H535–H543.
(15) Suttorp, N.; Hessz, T.; Seeger, W.; Wilke, A.; Koob, R.; Lutz, F.; Drenckhahn, D. *Am. J. Physiol.* **1988**, *255*, C368–C376.
(16) Weis, S. M.; Cheresh, D. A. *Nature* **2005**, *437*, 497–504.
(17) Youdim, K. A.; Avdeef, A.; Abbott, N. J. *Drug Discovery Today* **2003**, *8*, 997–1003.
(18) Biganzoli, E.; Cavenaghi, L. A.; Rossi, R.; Brunati, M. C.; Nolli, M. L. *Farmaco* **1999**, *54*, 594–599.
(19) Jo, H.; Dull, R. O.; Hollis, T. M.; Tarbell, J. M. *Am. J. Physiol.* **1991**, *260*, H1992–H1996.
(20) Yeon, J. H.; Park, J. K. *Anal. Chem.* **2009**, *81*, 1944–1951.
(21) Chueh, B. H.; Huh, D.; Kyrtsos, C. R.; Houssin, T.; Futai, N.; Takayama, S. *Anal. Chem.* **2007**, *79*, 3504–3508.
(22) Ismagilov, R. F.; Ng, J. M. K.; Kenis, P. J. A.; Whitesides, G. M. *Anal. Chem.* **2001**, *73*, 5207–5213.
(23) Neeves, K. B.; Diamond, S. L. *Lab Chip* **2008**, *8*, 701–709.
(24) Kuo, T. C.; Cannon, D. M.; Shannon, M. A.; Bohn, P. W.; Sweedler, J. V. *Sens. Actuators, A* **2003**, *102*, 223–233.
(25) Kimura, H.; Yamamoto, T.; Sakai, H.; Sakai, Y.; Fujii, T. *Lab Chip* **2008**, *8*, 741–746.
(26) Shao, J.; Wu, L.; Wu, J.; Zheng, Y.; Zhao, H.; Lou, X.; Jin, Q.; Zhao, J. *Biomed. Microdevices* [Online early access]. DOI: 10.1007/s10544-009-9362-0. Published Online: October 3, **2009**. http://www.springerlink.com/content/q1361477215vlh56/?p=3799173a7b904515a9758207547adbdc&pi=0.

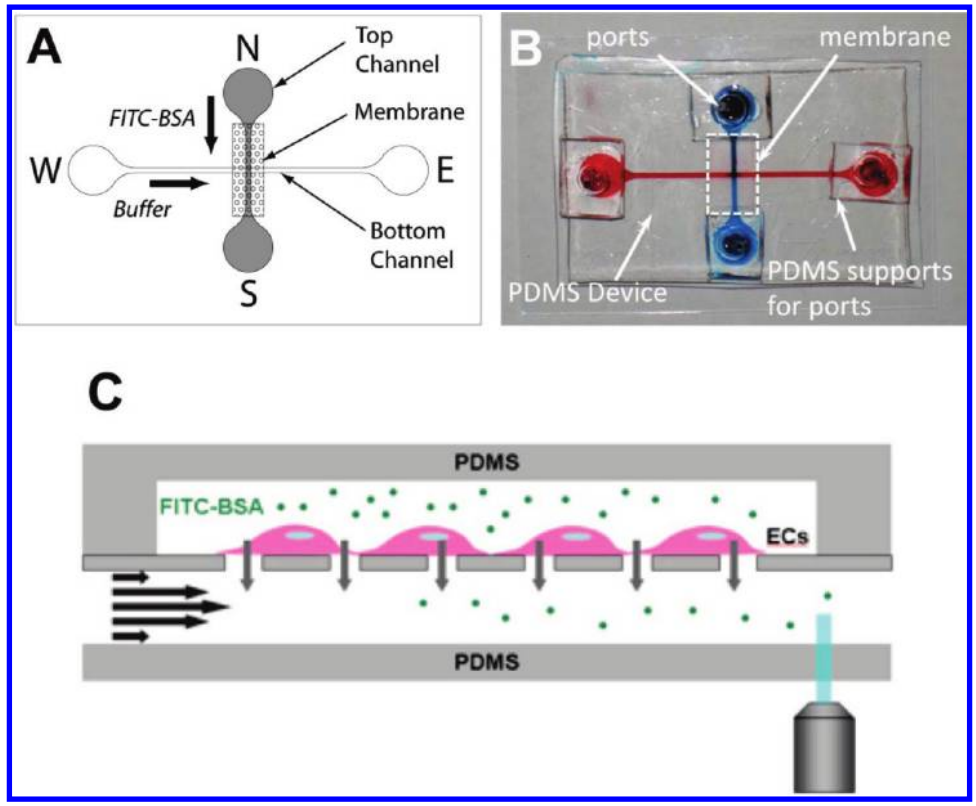

Figure 1. Two-layer membrane-based microfluidic system. (A) Illustration of microchannel cross pattern (top view). Polyester membrane (hatched) was sandwiched between the top north−south channel (gray) and bottom east−west channel (outline). Flow in the top channel was from N to S, and flow in the bottom channel was from W to E. (B) Photograph of the two-layer membrane device (top view). (C) Cross section of the microfluidic membrane device at the intersection of the top and bottom microchannels. FITC−BSA flows in the top channel (out of the page), then permeates the endothelial and membrane layers to the bottom channel, where a buffer stream carries the permeated analyte to a downstream detection point (bottom right).

reported in the literature.[21−24] PDMS was chosen for its ease of fabrication as well as for its optical properties.[27−29] All microchannels used in experiments were 100 μm deep by 800 μm wide. These dimensions were chosen to produce appropriate shear stresses over the range of practical flow rates and to provide enough surface area for cell growth and enough volume for microscale culture. Shear stresses ranging from 1 to 100 dyn/cm^2 can be applied using flow rates from 16 to 1600 μL/min, well within the limits of the syringe pump. Depending on the application, microchannel sizes can be easily modified to accommodate other experimental parameters of interest because of the convenience of soft lithography. Aspect ratios must be selected with caution, however, to ensure cell monolayers are exhibiting normal behaviors in morphology and function.

North−south and east−west channel patterns were drawn in AutoCAD and printed on a transparent photomask (City Graphics, Toronto, Canada). Masters and PDMS casts were fabricated as described previously.[7] After casting, PDMS slabs containing the channel features were carefully released from masters, rinsed with distilled water and isopropyl alcohol, and dried under nitrogen gas before membrane bonding. Top and bottom PDMS slabs were bonded to the membrane using the stamping procedure reported by Chueh et al.[21] Briefly, PDMS prepolymer (10:1 ratio of base to curing agent) was mixed with toluene in equal portions and spin-coated (500 rpm/s ramp for 4 s, 1500 rpm for 60 s) onto a clean glass slide to form a thin PDMS mortar film. On the basis of the report by Chueh et al., we estimated the mortar layer to be ~2−3 μm thick.[21] PDMS slabs were stamped onto the mortar film for 1 min and were then removed and positioned mortar-side up. Membrane edges were gently dipped onto mortar prior to placement at the intersection and bonding of the mortar-coated PDMS slabs. After assembly of the membrane and slabs, the device was placed in an oven at 70 °C overnight to cure the mortar. Inlet and outlet ports were inserted to provide connections to top and bottom microchannel reservoirs. The final device fit on a 75 mm × 50 mm glass slide (Figure 1B).

Cell Isolation and Culture. Primary porcine aortic endothelial cells (PAECs) were generously donated by Lowell Langille (University of Toronto). These cells were isolated from porcine thoracic aortas obtained from a local slaughterhouse using an isolation procedure similar to a previously described method.[30,31] PAECs were cultured in M199 supplemented with 5% fetal bovine serum (FBS), 5% cosmic calf serum (CS), and 1% penicillin−streptomycin (P−S) (PAEC media) at 37 °C with 5% CO_2. Cells were fed every other day and passaged every 3−4 days. All reported experiments used cells between passages 4 and 7.

(27) Piruska, A.; Nikcevic, I.; Lee, S. H.; Ahn, C.; Heineman, W. R.; Limbach, P. A.; Seliskar, C. J. *Lab Chip* **2005**, *5*, 1348–1354.
(28) Zeng, H. L.; Li, H. F.; Lin, J. M. *Anal. Chim. Acta* **2005**, *551*, 1–8.
(29) Llobera, A.; Demming, S.; Wilke, R.; Buttgenbach, S. *Lab Chip* **2007**, *7*, 1560–1566.
(30) Noria, S.; Cowan, D. B.; Gotlieb, A. I.; Langille, B. L. *Circ. Res.* **1999**, *85*, 504–514.
(31) Wong, M. K. K.; Gotlieb, A. I. *Lab. Invest.* **1984**, *51*, 75–81.

Cell Adhesion on Membrane. Various membranes were tested to determine the best membrane type for cell adhesion and growth. Cyclopore polycarbonate regular (PC-1), Cyclopore polycarbonate thin clear (PC-2), and Nuclepore polycarbonate (PC-3) track-etched membranes were purchased from Whatman Inc. (Florham Park, NJ) as individual membrane sheets. Poly(ethylene terephthalate) (PET) membranes were obtained by removing the membrane surface from the bottom of cell culture inserts (Becton Dickinson, Mississauga, ON, Canada). Glass coverslips were used as control for substrate type. All membranes tested had 1.0 μm diameter pores, which based on manufacturer's recommendations, are large enough to permit molecular transport but sufficiently small to prevent cell migration.

Membranes were trimmed into circular discs of ~12 mm diameter, dipped in 70% ethanol for sterilization, and carefully dried over a small flame. Dried membranes were placed in wells of a 12-well plate, and coated with fibronectin (FN) for 24 h. PAECs were seeded at 7500 cells/cm^2 and cultured for 2 days prior to fixation with neutral buffered formalin. Media was replaced after the first day of culture to remove unattached cells and replenish nutrients in the media. After fixation, cells were stained with Hoechst nuclear dye and phalloidin (filamentous actin) for cell counting and qualitative assessment of cell spreading on the membrane, respectively.

Fluorescent images were captured using a CCD camera (QImaging Retiga, Surrey, BC) connected to an inverted fluorescent microscope (Olympus IX-71). Three random images were taken per sample as representative of the overall coverage of cells on the membrane, and total number of cells per sample was counted. Three independent samples ($n = 3$) were analyzed, and the average total cell count was determined.

Two-way analysis of variance (ANOVA) was performed using SigmaStat to analyze the effects of membrane type (PC-1, PC-2, PC-3, PET, glass (control)) and protein coating (none, 25 μg/mL FN, 100 μg/mL FN), or any interaction between the two factors, on total cell count. No interaction between factors was found ($P > 0.05$). Tukey pairwise multiple comparisons were used to determine statistical significance between substrate groups.

Device Preparation and Cell Seeding. PAECs were cultured directly in membrane-based microfluidic systems for permeability experiments. Top and bottom microchannels were rinsed successively with ~1 mL of 100% ethanol, ~5 mL of 70% ethanol for sterilization, and ~5 mL of phosphate-buffered saline (PBS). Bovine plasma FN (Sigma-Aldrich Canada) at 100 or 200 μg/mL diluted in supplemented media was injected into the top microchannel and incubated at room temperature for 90 min to allow FN to adsorb onto the membrane surface. PAECs were trypsinized and suspended at a cell density of 0.5 to 4.0 $\times$ 10^6 cells/mL. PAECs were seeded into the top channel of the membrane device and allowed to attach to the FN-coated membrane surface during an initial 4−6 h static culture stage in an incubator maintained at 37 °C with 5% CO_2. Media in the microchannels was replenished by injecting 1 mL of media. Cells were subsequently maintained by perfusing media at 100 μL/h using a syringe pump for 4−5 days. Cells within the microchannels were incubated with 2 μM calcein AM and 4 μM ethidium homodimer-1 for 30 min to distinguish live and dead cells under fluorescence, respectively.

Laser-Induced Fluorescence Microscopy Setup. Permeability through membrane and cell layers was measured by flowing fluorescein isothiocyanate-labeled bovine serum albumin (FITC−BSA, 2 μg/mL in buffer unless otherwise noted) into the top channel and allowing FITC−BSA to pass through the cell layer and membrane to the bottom channel where it was mixed with a flowing buffer stream (Figure 1C). To reduce BSA adsorption in the device, M199 basal medium with 0.1% (w/v) Pluronic F68 (Sigma-Aldrich Canada) was used as buffer for all experiments. Top and bottom channel inlet ports were connected to syringe pumps (Harvard Apparatus, Holliston, MA) via polyethylene tubing. Laser-induced fluorescence (LIF) was used to detect FITC−BSA in the bottom channel. The 488 nm line of an argon ion laser (Melles Griot, Carlsbad, CA) was focused downstream of the membrane on the bottom channel using a 10× objective on an inverted microscope (Olympus IX-71). Fluorescence was captured by the same objective, filtered both optically (536/40 nm band-pass and 488 nm notch filter) and spatially (500 μm pinhole) and imaged onto a photomultiplier tube (PMT, Hammamatsu, Bridgewater, NJ). PMT current was converted to voltage by a picoammeter (Keithley Instruments, Cleveland, OH), and analog-to-digital conversion was performed by a data acquisition pad (National Instruments, Austin, TX) linked to a computer running custom acquisition software in LabVIEW (National Instruments).

Permeability Using LIF Detection. Permeability was determined by measuring inline fluorescence intensity at the point of optical detection, relating the fluorescence intensity to the ratio of solute concentration between top and bottom microchannels, and employing the classical Darcy's law for porous media flow. Details of the derivation for all modeling equations are included in the Supporting Information. We summarize the key equations here to facilitate discussion of results. Darcy's law predicts that the superficial velocity (i.e., the permeate flux per unit area), v_s, is governed by[32]

$$v_s = -\frac{k}{\mu}\frac{dp}{dz} = \frac{k}{\mu}\frac{\Delta p_T}{\delta} \tag{1}$$

where k is the permeability coefficient in (m^2), μ is the dynamic viscosity of the fluid in (N·s/m^2), and dp/dz is the pressure gradient across the membrane in (N/m^3). The pressure gradient is represented by the transmembrane pressure drop Δp_T across the thickness of the membrane δ. To determine the permeability coefficient k experimentally using the LIF setup, a combination of Darcy's law and mixing principles was employed. Transmembrane pressure was calculated by determining the pressure at the half-length of both top and bottom microchannels:

$$\Delta p_T = p_{t,m} - p_{b,m} = 6\mu\left(\frac{L_t v_t}{h_t^2} - \frac{L_b v_{b0}}{h_b^2}\right)\left(\frac{m+1}{m}\right) \tag{2}$$

(32) Scheidegger, A. E. *The Physics of Flow through Porous Media*; University of Toronto Press: Toronto, Canada, 1974.

In eq 2, m is an empirical constant that accounts for side wall effects in a channel with rectangular cross section,[33] v_t and v_{b0} are the average fluid velocities of the top and bottom channels, L_t and L_b are the top and bottom channel lengths, respectively, and h_t and h_b are the top and bottom channel heights, respectively.

The superficial velocity v_s was determined by considering the amount of fluorescent material permeating and mixing with the flowing buffer in the bottom channel. If concentration of FITC−BSA in the top channel is considered the maximum fluorescence intensity in the system (C_{max}), the concentration of FITC−BSA permeated through the membrane (C_f) and mixed into the buffer stream must be a fraction of the maximum, in a ratio ($\bar{C}$) that involves the volume of permeate from the top channel and the total volume of permeate plus buffer being mixed in the bottom channel:

$$\bar{C} = \frac{C_f}{C_{max}} = \frac{f_c v_s w_t}{v_s w_t + v_{b0} h_b} \tag{3}$$

where w_t is the width of the top microchannel. Although both convective and diffusive components of solute flux were considered in the derivation, eq 3 comprised only convective transport because our operating conditions yielded large pore Peclet number ($Pe_p > 200$), resulting in a negligible contribution from diffusive flux. f_c in the numerator represents a convective flux factor that accounts for secondary steric and viscous effects that affect solute flux through pores (see the Supporting Information). Rearranging eqs 1−3 yields a closed-form solution for k:

$$k = \frac{1}{6}\left[\frac{\bar{C}}{f_c - \bar{C}}\right]\left[\frac{h_t^2 h_b^3 \delta}{w_t}\right]\left[\frac{v_{b0}}{L_t v_t h_b^2 - L_b v_{b0} h_t^2}\right]\left[\frac{m}{m+1}\right] \tag{4}$$

Thus, permeability can be explicitly determined in real time by simply multiplying parameters of microchannel and membrane geometry, chosen flow rates, empirical constants, and detected fluorescent intensities (represented by normalized concentration values).

Permeability Measurements. Real-time permeability was measured using LIF detection, and calculated by applying the mixing model as described above. A typical experiment involved flowing FITC−BSA into the top microchannel at a constant flow rate and flowing buffer into the bottom microchannel over a range of flow rates in a stepwise manner (Figure 2). As bottom channel flow rate (Q_b) was adjusted, the measured fluorescence intensity changed as a result of corresponding changes in transmembrane pressure that led to differences in the amount of permeating FITC−BSA. Each experimental run started with an injection (via syringe) of FITC−BSA into both top and bottom microchannels. For normalization, fluorescence of this solution was measured at the detection point to establish maximum fluorescence for a particular run (t = 0−2.5 min of Figure 2). This corresponded to $\bar{C} = f_c \sim 1$ for $v_{b0} = 0$ μL/min

(33) Shah, R. K.; London, A. L. *Laminar Flow Forced Convection in Ducts*; Academic Press: New York, 1978.

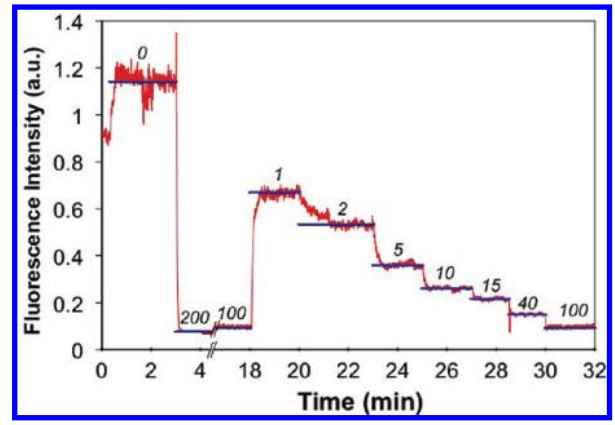

Figure 2. Fluorescence intensity vs time curve. A typical real-time fluorescence intensity curve for predicting albumin permeability was generated via LIF detection at a prescribed location downstream of the intersection. Top channel flow rate was held constant (v_t = 400 μL/min) while the bottom channel flow rate was ramped (v_{b0} = 0−200 μL/min, italicized numbers) to create a stepwise curve. Blue lines represent average fluorescence values in the plateau region for each step. The length of the blue line represents the length of time in which the particular flow rate was applied. (a.u. = arbitrary units (before normalization)).

in eq 3. To measure background fluorescence, top and bottom channel flow rates were chosen to yield zero transmembrane pressure, which corresponded to no flow through membrane, or $v_s = 0$ by eq 1. For example, because L_t = 25 mm and L_b = 50 mm for our devices, the combination of v_t = 400 μL/min and v_{b0} = 200 μL/min yielded zero transmembrane pressure according to eq 2 (nonzero but negligible transmembrane pressure in practice). This was captured in Figure 2 as the baseline fluorescence at time t = 3−4.5 min where v_{b0} = 200 μL/min yielded the lowest detectable fluorescence. Using these measurements as maximum and minimum markers for each run, we normalized all intensities to fall between $\bar{C} = 0$ and $\bar{C} = 1$.

Averaged fluorescence intensity measurements at plateau regions were normalized to maximum fluorescence intensity and plotted versus flow rate ratio, defined as $R = Q_t/Q_b$. R is a surrogate variable for bottom channel flow rate because Q_t is constant in the devised procedure. A curve-fitting procedure using Darcy's law and the mixing model (eqs 1 and 3) was employed to extract a predicted permeability coefficient k from the experimental curve. Specifically, a theoretical value k_0 was guessed to produce superficial velocities and normalized concentrations at each data point on the curve (for each of n tested flow rate ratios), based on k_0, i.e.,

$$v_{s,i} = \frac{k_0}{\mu}\frac{(\Delta p_T)_i}{\delta}, \quad i = 1, 2, ..., n \tag{5}$$

and

$$\bar{C}_{t,i} = \frac{f_c v_{s,i} w_t}{v_{s,i} w_t + v_{b0,i} h_b}, \quad i = 1, 2, ..., n \tag{6}$$

where $v_{s,i}$, $(\Delta p_T)_i$, $v_{b0,i}$, and $\bar{C}_{t,i}$ were the superficial velocity, transmembrane pressure, bottom channel flow rate, and normalized concentrations for the ith of n flow rate ratios. The

theoretical value $\bar{C}_{t,i}$ from eq 6 was then compared to normalized fluorescence intensities from experiment, $\bar{C}_{e,i}$, at each flow rate ratio R_i, and a sum of squares of differences, $S(k_0)$, was determined by

$$S(k_0) = \sum_i (\bar{C}_{t,i} - \bar{C}_{e,i})^2 \quad (7)$$

The k_0 value that yielded the minimum of $S(k_0)$ was considered the experimental permeability coefficient.

RESULTS AND DISCUSSION

Cell Adhesion on Membranes. Membranes were tested for cell adhesion and growth by culturing PAECs on protein-coated or noncoated surfaces and counting the number of total adhered cells in representative images. Cells were cultured for 2 days on these surfaces in wells to allow enough time for cells to proliferate after attachment. After fixation, cells were stained with Hoechst nuclear dye to label the nuclei for cell counting and phalloidin to label actin stress fibres for qualitative assessment of overall cell spreading. PAECs did not attach well to any of the polycarbonate membranes, especially when little or no protein was used (Figure 3). For 100 μg/mL FN, PAECs attached and spread only minimally, with only a small area covered by cells. Cell shape on these membranes was also not indicative of typical EC cultures having polygonal cell bodies and cobblestone morphology. On the other hand, PAECs displayed adhesion and growth on PET membranes for all protein-coated surfaces similar to that seen on glass coverslips. Even without protein coating, cells attached to the membrane and formed EC islands. With 100 μg/mL FN, PAECs covered large regions of the membrane and reached full confluence in these areas, similar to glass. There were no statistical differences in adhesion between cells grown on PET membrane and glass ($P > 0.5$), but a significant difference between cells grown on PET and polycarbonate membranes ($P < 0.01$) (Figure 3). Thus, we chose PET membranes for all subsequent experimentation involving cell culture on membranes. In some cases, ECs did not achieve full confluence over the entire PET membrane, likely due to nonuniformity of the FN coating, which was confirmed by immunostaining (data not shown). The advantage of using PET membranes, however, is that they can be modified to enhance protein coating using, for example, 3-aminopropyltriethoxysilane (APTES) in conjunction with glutaraldehyde (GA) to provide an aldehyde group for covalent bonding with amine groups of proteins.[34] APTES−GA chemistry has previously been used to immobilize proteins via this imine linkage,[35] and presumably this surface modification would allow for uniform immobilization of FN to the membranes to improve uniformity of endothelial coverage.

Device Characterization. Fabricated membrane devices were visually inspected to ensure proper sealing of the membrane between the PDMS casts. Occasionally, devices were observed to have air bubbles trapped near the membrane edges and were not used. To confirm proper device operation during permeability tests, fluorescent video microscopy was used to test membrane reliability and fidelity of the leak-free devices (see Figure S-1 in the Supporting Information). Top and bottom microchannels were first filled with 10 mM PBS with 0.05% (w/v) Pluronic F-68 (buffer) to prime the device. Pluronic additives were previously shown to reduce fouling on hydrophobic microfluidic device surfaces.[36] We confirmed in preliminary experiments that PAECs grown on tissue culture-treated polystyrene and cultured with 0.1% (w/v) Pluronic F68 added to supplemented M199 media remained viable for up to a week, with no noticeable changes in morphology (data not shown).

Minimization of fouling was important because FITC−BSA (and albumin in general) is a hydrophobic macromolecule (~66 kDa) that tends to adsorb to other hydrophobic surfaces like PDMS. Since FITC−BSA (Stokes radius ~4 nm) is much smaller than the 1 μm diameter cylindrical pores of the membrane, it readily diffuses through the membrane pores. In vivo, transport of albumin occurs either transcellularly via vesicle carriers under normal conditions or via both transcellular and paracellular pathways under pathologic conditions linked to endothelial dysfunction (e.g., inflammation).[37] This is in contrast to the transport of fluorescein alone (~400 Da), which has been shown to occur transcellularly through Caco-2 cells via monocarboxylic acid transporters,[38] as well as through endothelial cells of the blood−brain barrier via organic anion transporters.[39]

FITC−BSA (2 μg/mL in buffer) was manually injected into the top channel via syringe and allowed to permeate the membrane at the channel intersection. Permeation was a result of positive transmembrane pressure generated by flow in the top channel with no flow in the bottom channel. After less than a minute of permeation and noticeable accumulation of FITC−BSA in the bottom channel, flow was switched such that buffer was injected into the bottom channel while flow was ceased in the top channel. The accumulated dye molecules washed downstream as expected. Furthermore, because of the switch in flows, transmembrane pressure from bottom to top channel resulted in permeation of buffer through the membrane into the top channel. This washed away FITC−BSA in the top channel in both the upstream and downstream directions from the intersection. The addition of Pluronic F-68 in the buffer solution significantly reduced membrane fouling due to BSA adsorption. These characterization steps further confirmed that the fabricated devices were free of leakages, and flow between microchannels was strictly through membrane pores.

Viability of Cultured Cells. Cells seeded and cultured in membrane microfluidic devices were perfused at flow rates of 100 μL/h, which generated an average shear stress of ~0.15 dyn/cm^2. This shear stress was too low to detach cells or induce shear-related responses. Cells were monitored for viability and proliferation by calcein AM/ethidium homodimer-1 staining every 24 h. Cells attached, spread, and proliferated to near confluence over 4−5 days. Cells were 100% viable under these conditions for the duration of culture (Figure 4).

Permeability Measurements. Figure 2 shows typical readings from LIF detection during the stepwise procedure where

(34) Bui, L. N.; Thompson, M.; McKeown, N. B.; Romaschin, A. D.; Kalman, P. G. *Analyst* **1993**, *118*, 463–474.
(35) Wang, Z. H.; Jin, G. *J. Immunol. Methods* **2004**, *285*, 237–243.
(36) Luk, V. N.; Mo, G. C. H.; Wheeler, A. R. *Langmuir* **2008**, *24*, 6382–6389.
(37) Hu, G. C.; Place, A. T.; Minshall, R. D. *Chem.−Biol. Interact.* **2008**, *171*, 177–189.
(38) Kuwayama, K.; Miyauchi, S.; Tateoka, R.; Abe, H.; Kamo, N. *Biochem. Pharmacol.* **2002**, *63*, 81–88.
(39) Sun, H. Y.; Miller, D. W.; Elmquist, W. F. *Pharm. Res.* **2001**, *18*, 1542–1549.

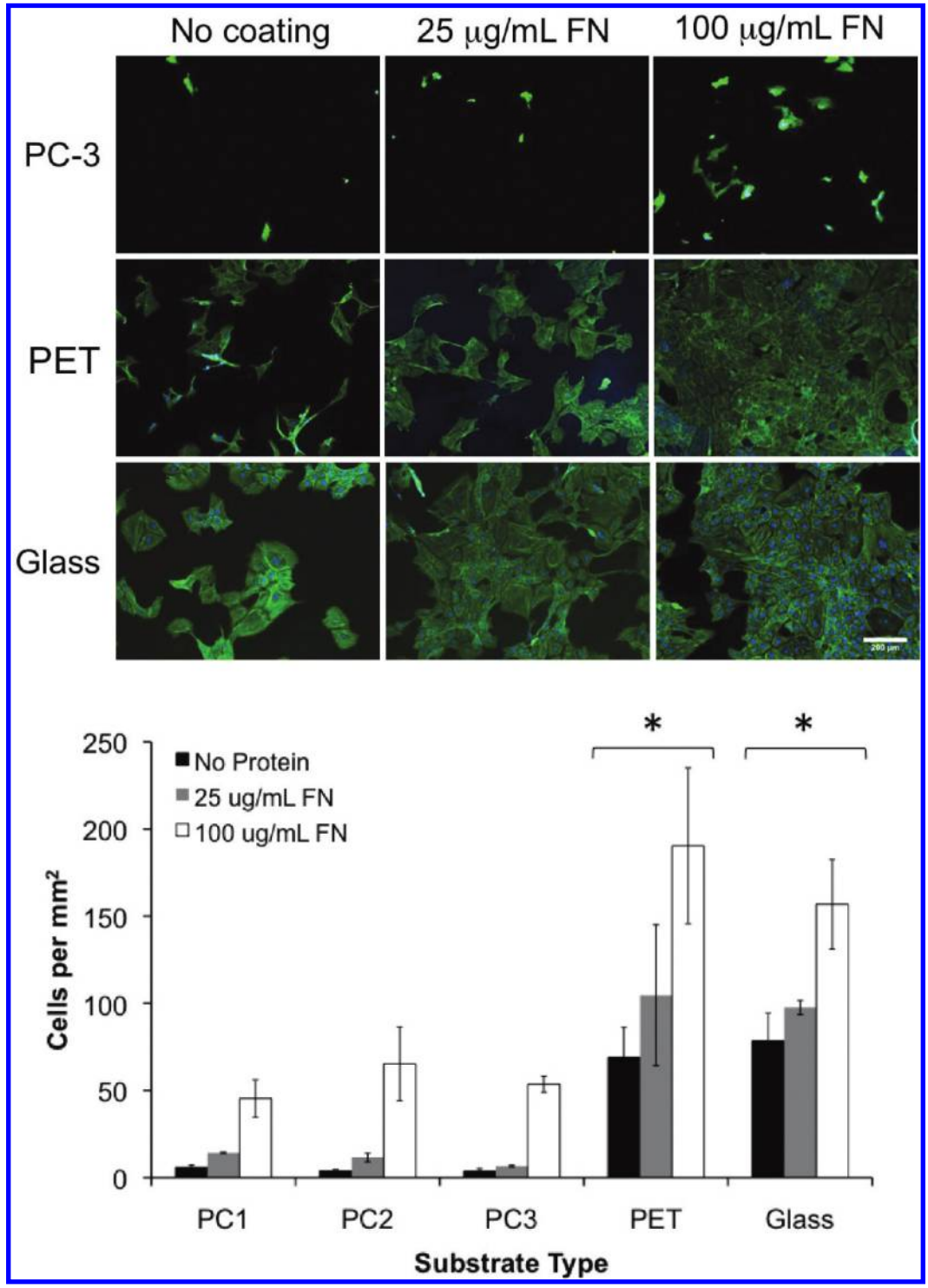

Figure 3. PAEC adhesion on protein-coated membranes. Phalloidin-stained (green) PAECs after 24 h of static culture on protein-coated membranes. Glass was used as a positive control. PET membranes promoted adhesion and growth similar to glass and yielded the most confluent monolayers among all membranes tested. Scale bar = 200 μm (bottom right). Results were quantified as cell counts per unit area for all substrates. Statistical significance (* $P < 0.05$) was found for the PET membrane against all other membrane substrates and for glass against all other membrane substrates.

bottom channel flow rates were adjusted. As flow rates were changed (e.g., from 100 to 1 μL/min at $t = 18$ min, from 1 to 2 μL/min at $t = 20$ min, and from 2 to 5 μL/min at $t = 23$ min), the detected fluorescence intensities changed accordingly through a transient stage before reaching a plateau. At higher bottom channel flow rates, the transient stage was shorter in time. A 30 s average of an arbitrarily chosen portion of the plateau region was taken as the representative intensity measurement at that flow rate (blue lines in Figure 2). Multiple cycles of the stepwise procedure with good repeatability are possible during one experiment depending on the volume of syringes used. Figure 2 displays the second cycle of a two-cycle run, where the first cycle from t

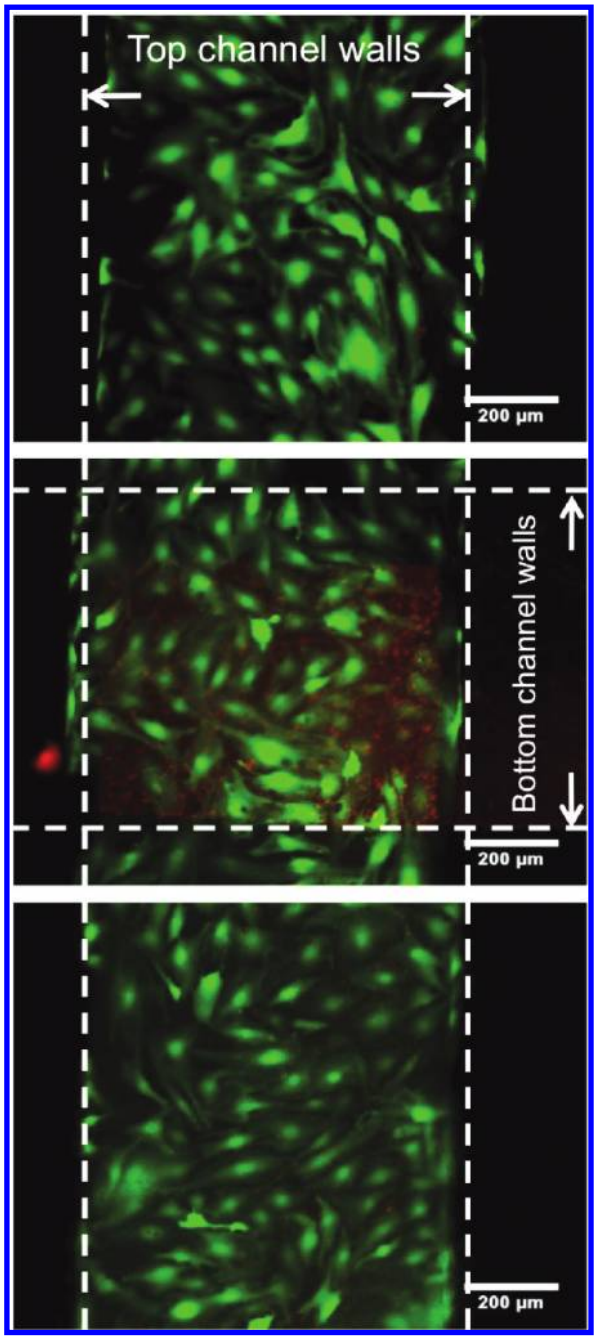

Figure 4. Calcein AM/ethidium homodimer-1 staining of live PAECs during perfusion culture. Views of the cells in the top channel after 4 days of perfusion culture. The three panels represent adjacent regions of the top channel. The middle panel shows the intersection of the top and bottom channels, with dotted white lines delineating the channel walls. Perfusion was at 100 μL/h from the top panel to the bottom panel. Cells reached confluence after 4 or 5 days, with some regions lacking cell−cell contacts. Calcien AM (green cytoplasm) and ethidium homodimer (red nuclei). Scale bar = 200 μm.

= 4.5 min to t = 16.5 min was truncated for clarity. As bottom channel flow rate increased, detected fluorescence intensity decreased. This was expected from eq 3 since higher v_{b0} meant the permeated molecules were more diluted by the time it reached the detection point.

Figure 5 shows representative curves of normalized fluorescence intensities versus flow rate ratio for three experimental cases: (1) for the 1 μm nominal pore size PET membrane alone

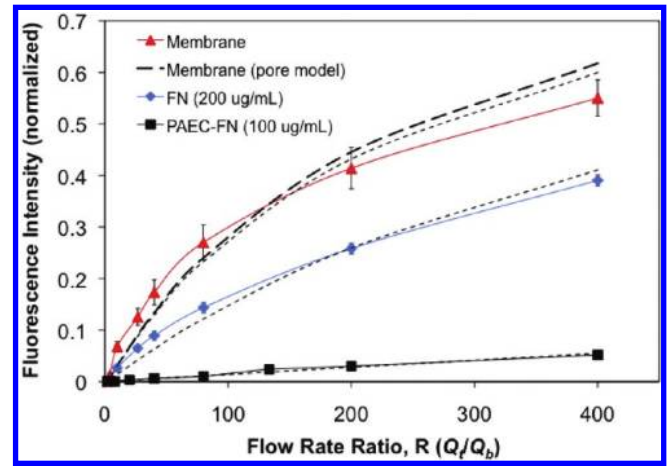

Figure 5. Normalized fluorescence intensity vs flow rate ratio. Fluorescence intensity decreased with lower flow rate ratio (or higher Q_b): membrane alone (red), FN-coated membrane (200 μg/mL) (blue), and PAECs grown on FN-coated membrane (100 μg/mL) (black solid). The theoretical curve for the membrane alone, using the cylindrical pore model (black dashed), was in excellent agreement with the measured curve for the membrane alone. Dotted lines are curve fits through experimental curves. Each curve represents results from one device. Error bars = SE; $n \geq 3$ measured plateau regions for each flow rate ratio. PAEC-FN data for $n = 1$ only.

(red line), (2) for PET membrane coated with 200 μg/mL FN (blue line), and (3) for fixed PAECs grown to confluence on FN-coated membrane (black line). All three curves showed trends that reflected those of the time curves, where increasing bottom channel flow rate (or decreasing R) led to decreasing fluorescence intensity. For a given flow rate ratio, the membrane alone was the most permeable (highest fluorescence intensity), followed by the FN-coated membrane, and the PAECs on FN-coated membrane (lowest fluorescence intensity), as expected. A theoretical curve was also plotted for the membrane alone (black dashed line of Figure 5) based on the cylindrical pore model (i.e., $k_0 = n\pi r_p^4/8$) and a measured pore density and pore radius of n = 17 700 pores/mm^2 and r = 0.54 μm, respectively, as determined by scanning electron microscopy (see the Supporting Information). The theoretical curve matched the experimental measurement for k through an untreated membrane with excellent agreement (<1% error between theory ($k = 5.77 \times 10^{-10}$ mm^2) and measurement ($k = 5.73 \times 10^{-10}$ mm^2)) when secondary steric and viscous effects were considered.[40]

Permeability coefficients from curve fits were calculated and compared to several related results from the literature. These other studies reported permeability coefficients as hydraulic conductivity L_p (cm·s^{-1}·cmH$_2$O^{-1}), which is directly proportional to k. In our experiments, PAECs grown on FN were exposed to shear of 25 dyn/cm^2. The various reports from literature were for permeability tests on ECs with and without shear. Comparisons show that our results for fixed PAECs grown on FN (k = 21.4 nm^2; $L_p = 19.1 \times 10^{-6}$ cm·s^{-1}·cmH$_2$O^{-1}) were approximately 1 order of magnitude higher than results for both fixed pulmonary artery ECs ($L_p = 1.1 \times 10^{-6}$),[41] as well as for live bovine aortic ECs after 5 h of thrombin induction

(40) Friedman, M. H. *Principles and Models of Biological Transport*; Springer: New York, 2008.
(41) Turner, M. R. *J. Physiol. (London)* **1992**, *449*, 1–20.

($L_p = 2.4 \times 10^{-6}$),[14] but were 1 order of magnitude lower than without cells (FN-coated membrane) ($k = 261$ nm^2), as expected. These results suggest that our method produces reasonable permeability values for sheared ECs. In particular, the presence of the subconfluent EC monolayer in our study significantly reduced overall permeability compared to endothelial-free membrane layers. The most likely causes of the discrepancy between our data and those from previous experiments were the high shear stress applied in our experiments (shear stress increases permeability[14]) and the lack of a fully confluent monolayer. As mentioned, the application of shear stress on the endothelium is important for measurements of vascular permeability. The current microfluidic device allowed for precise control of the flow-induced shear on the culture endothelial layer and does so with a much smaller platform in comparison to traditional setups.[14,19] Although the device is also capable of measuring active transport under static conditions, the most important benefit comes from the simultaneous application of shear and direct online detection of analyte. Online detection in the current setup requires fluorescently labeled molecules, but other analytical methods such as liquid chromatography could be used for compounds whose physicochemical properties may be substantially altered by dye labeling.[20] Although confluent endothelial monolayers represent conditions of vascular homeostasis in vivo, subconfluent endothelial monolayers are importantly associated with conditions of pathophysiology that are characterized by loss of cell−cell contacts between ECs, increased gap distance between interendothelial junctions,[42] and ultimately higher vascular permeability. Studying the permeability of compromised or "leaky" endothelial monolayers is critical to furthering our understanding of disease development, particularly since increased vascular permeability is implicated in diseases that include neuropathologies,[43] cancer metastasis,[44] ischemia, and other cardiovascular diseases.[16]

CONCLUSIONS

In summary, the membrane-based microfluidic device and model-based experimental scheme enabled endothelial permeability measurements under shear stress conditions. The device is flexible to the needs of the researcher because modifications can be made to channel dimensions via soft lithography and to the membrane surface via standard surface chemistry. Live cells can be exposed to appropriate shear stresses, and throughput can be increased significantly with parallelization.

ACKNOWLEDGMENT

The authors acknowledge the financial support from the Ontario Graduate Scholarship Program (M.W.L.W. and S.S.), a Grant-in-Aid (NA 6047) from the Heart and Stroke Foundation of Ontario (C.A.S.), the Ontario Early Researcher Award (C.A.S.), and the Canada Research Chairs in Mechanobiology (C.A.S.) and Bioanalytical Chemistry (A.R.W.).

SUPPORTING INFORMATION AVAILABLE

Additional information as noted in text. This material is available free of charge via the Internet at http://pubs.acs.org.

Received for review July 14, 2009. Accepted November 30, 2009.

AC901560W

(42) Knezevic, I. I.; Predescu, S. A.; Neamu, R. F.; Gorovoy, M. S.; Knezevic, N. M.; Easington, C.; Malik, A. B.; Predescu, D. N. *J. Biol. Chem.* **2009**, *284*, 5381–5394.

(43) Huber, J. D.; Egleton, R. D.; Davis, T. P. *Trends Neurosci.* **2001**, *24*, 719–725.

(44) Martin, T. A.; Jiang, W. G. *Histol. Histopathol.* **2001**, *16*, 1183–1195.